Anisotropic Chemical Shielding, M-Site Ordering, and Characterization of Extraframework Cations in ETS-10 Studied through MAS/MQ-MAS NMR and Molecular Modeling Techniques

S. Ganapathy,*,† T. K. Das,† R. Vetrivel,† S. S. Ray,† T. Sen,† S. Sivasanker,*,† L. Delevoye,‡ C. Fernandez,‡ and J. P. Amoureux‡

Contribution from the National Chemical Laboratory, Pune - 411 008, India, and Laboratoire de Dynamique et Structure des Materiaux Moleculaires, CNRS URA 801, Université des Sciences et Technologies de Lille, F-59655 Villeneuve D'ASCQ Cedex, France

Received August 5, 1997

Abstract: The local structural characteristics of Si and Ti sites in ETS-10 as derived from a combination of high-resolution magic angle spinning (MAS) NMR spectroscopic and molecular modeling studies are reported. Pure and highly crystalline ETS-10 and aluminum-substituted ETS-10 (ETAS-10), devoid of impurity ETS-4 phase, were synthesized and fully studied by MAS and multiple-quantum magic angle spinning (MQ-MAS) NMR. More accurate assignments of the experimentally observed ^{29}Si resonances to the crystallographically nonequivalent Si sites are made, and a correlation with T-site geometry is established. ^{29}Si slow MAS NMR is shown to be a very general and powerful methodology to unequivocally establish heteroatom substitution in the zeolite lattice, and this was used to probe the local symmetry and chemical shielding at different Si sites in ETS-10 and ETAS-10. ^{29}Si and ^{27}Al MAS NMR spectral analysis of ETAS-10 is used to confirm that the aluminum substitution occurs only in Si[4Si,0Ti] silicon sites. This, in turn, was used to generate cluster models for computer graphics techniques. The electronic structure of such cluster models and the calculated aluminum substitution energy values pinpoint the topographical location of aluminum in ETAS-10. The acidity of ETAS-10 is predicted on the basis of the quantum chemical cluster model calculations. The first application of MQ-MAS NMR to study cation environments in molecular sieves is also reported and is used in the present study to investigate the local structural characteristics of sodium cations in ETS-10 and ETAS-10.

Introduction

An industrially significant discovery is the titanosilicate (TS-1) with MFI framework structure,[1] which is constructed of linked SiO_4 tetrahedra and TiO_4 tetrahedra. Though it is widely accepted that Ti is in a distorted tetrahedral coordination, there are differences of opinion regarding the extent of distortion. It has been pointed out by On Trong et al.[2] that the distortion is so high that the Ti ions cannot be considered anymore as part of the framework. However, Bellusi and Fattore[3] argued that the distortion is minimal and hence titanium can be assumed to be in the framework. The dispute has not been solved because the concentration of the titanium is too low (Si/Ti = 30) to be characterized by any bulk analytical techniques and the coordination around Ti is so labile that it depends on the experimental conditions.

ETS-10 is a prominent member of a microporous titanosilicate family whose basic structural characteristics comprise corner-sharing SiO_4 tetrahedra and TiO_6 octahedra linked through bridging oxygens. Although it has been just recently discovered, there have been a large number of studies[4−40] due to its interesting structural features. The pore system of ETS-10 has a stacking disorder,[17,18,24] comprising two ordered polymorphs,

* Corresponding authors. E-mail: siva@ems.ncl.res.in. or ganpat@ems.ncl.res.in. Fax: +91-212-334761/330233.

† National Chemical Laboratory.

‡ Universite des Sciences et Technologies de Lille.

(1) Taramasso, M.; Perego, G.; Notari, B. U.S. Patent 4,410,501, 1983.
(2) On Trong, D.; Bittar, A.; Sayari, A.; Kaliaguine, S.; Bonneviot, L. *Catal. Lett.* **1992**, *16*, 85.
(3) Bellussi, G.; Fattore, V. *Stud. Surf. Sci. Catal.* **1991**, *69*, 79−92.
(4) Kuznicki, S. M. Indian Pat. 171379, 1988.
(5) Kuznicki, S. M. Indian Pat. 171483, 1988.
(6) Kuznicki, S. M. U.S. Patent 4,853,202, 1989.
(7) Kuznicki, S. M.; Thrush, K. A. Eur. Pat. 0405978A1, 1990.
(8) Kuznicki, S. M. U.S. Patent 5,011,591, 1991.
(9) Kuznicki, S. M.; Thrush, K. A. U.S. Patent 4,994,191, 1991.
(10) Sommerfeld, D. A.; Ellis, W. R., Jr.; Eyring, E. M.; Kuznicki, S. M.; Thrush, K. A. *J. Phys. Chem.* **1992**, *96*, 9975−9978.
(11) Kuznicki, S. M.; Thrush, K. A.; Allen, F. M.; Levine, S. M.; Hamil, M. M.; Hayhurst, D. T.; Mansour, M. *Synth. Microporous Mater.* **1992**, *1*, 427−453.
(12) Kuznicki, S. M.; Thrush, K. A. U.S. Patent 5,208,006, 1993.
(13) Garfinkel, H. M.; Kuznicki, S. M.; Thrush, K. A. WO Pat. 9300152, 1993; EP Pat. 544892, 1993.
(14) Bozhilov, K. N.; Valtchev, V. *Mater. Res. Bull.* **1993**, *28*, 1209−1214.
(15) Review article: Looming Ban on Production of CFCs, Halons Spurs Switch to Substitutes. *Chem. Eng. News* **1993** (Nov. 15), 12−18.
(16) Kuznicki, S. M.; Dang, D.; Hayhurst, D. T.; Thrush, K. A. U.S. Patent 5,346,535, 1994.
(17) Anderson, M. W.; Terasaki, O.; Ohsuna, T.; Philippou, A.; Mackay, S. P.; Ferreira, A.; Rocha, J.; Lidin, S. *Nature* **1994**, *367*, 347−351.
(18) Ohuna, T.; Terasaki, O.; Watanabe, D.; Anderson, M. W.; Lidin, S. *Stud. Surf. Sci. Catal.* **1994**, *84*, 413−420.
(19) Das, T. K.; Chandwadkar, A. J.; Sivasanker, S. *Mater. Res. Bull.* **1994**, *17*, 1143−1153.
(20) Deeba, M.; Keweshan, C. F.; Koermer, G. S.; Kuznicki, S. M.; Madon, R. S. *Catalysis of Organic Reactions*; Kosak, J. R., Johnson, T. A., Eds.; Marcel Dekker Inc.: New York, 1994; pp 383−396.
(21) Valtchev, V. *J. Chem. Soc., Chem. Commun.* **1994**, 261−262.
(22) Valtchev, V.; Mintova, S. *Zeolites* **1994**, *14*, 697−700.
(23) Blosser, P. W.; Kuznicki, S. M. U.S. Patent 5,453,263, 1995.
(24) Anderson, M. W.; Terasaki, O.; Ohsuna, T.; Malley, P. J. O.; Philippou, A.; Mackay, S. P.; Ferreira, A.; Rocha, J.; Lidin, S. *Philos. Mag. B* **1995**, *71*, 813−841.
(25) Das, T. K.; Chandwadkar, A. J.; Budhkar, A. P.; Belhekar, A. A.; Sivasanker, S. *Microporous Mater.* **1995**, *4*, 195−203.

S0002-7863(97)02714-5 CCC: $15.00
Published on Web 05/02/1998

termed A and B.[17,24] It is titanium-rich (Si/Ti = 5) and is also the first microporous material wherein the location and coordination of metal atom, namely titanium, has been established from crystallographic and related techniques.[17,24] For a better utilization of newer materials (such as ETS-10) for molecular sieving and catalytic applications, it is essential to devise efficient and simple synthesis procedures and understand the structural features such as T-site ordering, as well as evaluate its electronic properties and acidity characteristics. Our paper focuses on the above aspects of ETS-10 through magic angle spinning (MAS) NMR, multiple-quantum magic angle spinning (MQ-MAS) NMR, and molecular modeling studies.

From the MAS NMR point of view, contrary to aluminosilicates,[41] the titanosilicate framework does not lead to dipolar broadening of the silicon lines since titanium can be considered to be magnetically dilute (^{47}Ti, ^{49}Ti; n = 7.28, 5.51%). Thus, the ^{29}Si MAS NMR spectra can be obtained at high magnetic fields (ca. 7 T) with increased resolution even for a very low value of Si/Ti, and additionally, they are readily amenable for a slow MAS spectral analysis to characterize the anisotropic chemical shielding and local symmetry at the various silicon sites. As shown in this paper, this approach is very general and therefore is useful in resolving disputes regarding heteroatom substitutions in the frameworks of microporous materials. Further, the recently discovered[42] MQ-MAS NMR techniques offer new opportunities to probe the sodium cation environment through ^{23}Na 3Q MAS and the aluminum substitution through ^{27}Al 3Q and 5Q MAS NMR.

We reported recently an efficient synthesis procedure for getting crystalline ETS-10 devoid of ETS-4 impurity.[31] We now report the structural and electronic characteristics of ETS-10 derived from high-resolution MAS NMR spectroscopy and molecular modeling techniques. ETS-10 is known to exist in two polymorphic forms A and B as reported by Anderson et al.[17,24] All our simulations, modeling, and the interpretation of the MAS NMR results are based on the crystal structure of polymorph B. The 80 silicon atoms in the unit cell of ETS-10 fall either into 11 types of Si sites in polymorph B or into 20 types of Si sites in the case of polymorph A. Thus our interpretation of results for polymorph B is applicable to polymorph A also, since the correspondence of the Si sites between the two polymorphs is known.[17,24] The as-synthesized ETS-10 is highly crystalline and has exceptional phase purity as observed from an enhanced signal multiplicity in ^{29}Si MAS experiments. Details of T-site ordering, cation site characterization, the framework substitution, and the favorable location of aluminum substitutions and acidity of ETAS-10 are reported here.

Experimental Section

Synthesis. Different methods of preparation of ETS-10 have been reported in the literature based on the titanium compounds used as the source of titanium. We recently reported a method for rapidly synthesizing ETS-10 in a highly crystalline and pure form.[31] The hydrothermal synthesis of ETS-10 using $TiCl_4$ was carried out with a gel of the following molar composition:

$$3.70Na_2O{:}0.95K_2O{:}TiO_2{:}5.71SiO_2{:}171H_2O$$

In a typical synthesis, a solution of 9.3 g of NaOH in 40 g of distilled water was added to a vigorously stirred solution of 52.5 g of sodium silicate (28.6% SiO_2, 8.82% Na_2O, 62.58% H_2O) and 40 g of distilled water. This was followed by the dropwise addition of 32.75 g of a $TiCl_4$ solution (25.42 wt % $TiCl_4$, 25.92 wt % HCl, 48.60 wt % H_2O) to this mixture (colorless gel) with rapid stirring. $KF{\cdot}2H_2O$ (7.8 g) was next added to the above gel (pH = 11.2 ± 0.1) and the mixture stirred well. The mixture was then transferred to a stirred stainless steel autoclave (Parr Instruments, U.S.) and the crystallization carried out at 473 K with a stirrer speed of 300 rpm for 16 h. After crystallization, the products were filtered and washed with deionized water until the pH of the filtrate was 10.7−10.8. It was dried at 373 K for 8−10 h. In earlier procedures, where $TiCl_3$ was the source of titanium,[17,19,24−27,33−35] ETS-4 or ETS-10 needed to be used as seed. Further, the crystallization time was long (many days) and the product invariably contained ETS-4 impurity.

ETAS-10 was synthesized using the same starting materials as ETS-10 except that a certain amount of sodium aluminate was added to the gel to get the desired Si/Al ratio in the product, the synthesis conditions being the same as above. Three samples with Si/Al ratios 62, 42, and 22 were synthesized.

MAS/MQ-MAS NMR Spectroscopy. MAS NMR spectra were recorded on a Bruker MSL-300 Fourier transform (FT) NMR spectrometer at ambient probe temperature (298 K). ^{29}Si NMR spectra were recorded at 59.621 MHz, while ^{27}Al NMR spectra were recorded at 78.206 MHz. The spinning speed was controlled to within ±5 Hz using a Bruker pneumatic speed controller. The magnetic field was carefully shimmed on the ^{1}H resonance sample of spinning TMS, which was subsequently used as external reference for ^{29}Si. The magic angle was precisely set using KBr and maximizing the rotational echo intensities of the satellite transitions of ^{79}Br. Free induction decays were accumulated in a 18-kHz spectral window using a 45° flip angle, 3-μs pulse, and 4-s relaxation delay. Typically, 8000−12 000 transients were accumulated before they were remotely processed on a SiliconGraphics Indigo2 workstation using the Bruker UXNMR software package.[43]

MQ-MAS NMR experiments were performed on a Bruker ASX-400 FT-NMR spectrometer equipped with a specially made MAS probehead capable of high-speed spinning (up to 15 kHz) and radio frequency field (rf) generation (up to 350 kHz). A three-pulse sequence, which incorporates a zero-quantum filter, was used. This pulse scheme ensures optimum selection of the mirror echo and anti-echo coherence transfer pathways to give pure absorption mode line shapes in the final two-dimensional (2D) SQ-MQ correlation plot. The first pulse was individually optimized for the 3Q (^{23}Na and ^{27}Al) experiments to obtain the best efficiency for the multiple-quantum (±3Q) coherence creation. In a similar way, the second pulse, which transfers these two symmetrical coherences into ZQ coherence, was also optimized. The further conversion to (−1Q) single-quantum coherence of the observed

(26) Rocha, J.; Lin, Z.; Ferreira, A.; Anderson, M. W. *J. Chem. Soc., Chem. Commun.* **1995**, 867−868.
(27) Anderson, M. W.; Philippou, A.; Lin, Z.; Ferreira, A.; Rocha, J. *Angew. Chem., Int. Ed. Engl.* **1995**, *34*, 1003−1005.
(28) Davis, R. J.; Liu, Z.; Tabora, J. E.; Wieland, W. S. *Catal. Lett.* **1995**, *34*, 101−113.
(29) Carli, R.; Bianchi, C. L.; Ragaini, V. *Catal. Lett.* **1995**, *33*, 49−55.
(30) Robert, R.; Rajmohanan, P. R.; Hegde, S. G.; Chandwadkar, A. J.; Ratnasamy, P. *J. Catal.* **1995**, *155*, 345−352.
(31) Das, T. K.; Chandwadkar, A. J.; Sivasanker, S. *J. Chem. Soc., Chem. Commun.* **1996**, 1105−1106.
(32) Sankar, G.; Bell, R. G.; Thomas, J. M.; Anderson, M. W.; Wright, P. A.; Rocha, J. *J. Phys. Chem.* **1996**, *100*, 449−452.
(33) Anderson, M. W.; Rocha, J.; Lin, Z.; Philippou, A.; Orion, I.; Ferreira, A. *Microporous Mater.* **1996**, *6*, 195−204.
(34) Das, T. K.; Chandwadkar, A. J.; Budhkar, A. P.; Sivasanker, S. *Microporous Mater.* **1996**, *5*, 401−410.
(35) Das, T. K.; Chandwadkar, A. J.; Sivasanker, S. *J. Mol. Catal.* **1996**, *107*, 199−205.
(36) Grillo, M. E.; Carrazza, J. *J. Phys. Chem.* **1996**, *100*, 12261−12264.
(37) Mihailova, B.; Valchev, V.; Mintova, S.; Konstantinov, L. *Zeolites* **1996**, *16*, 22−24.
(38) Yang, X.; Truitt, R. E. *J. Phys. Chem.* **1996**, *100*, 3713−3718.
(39) Liu, X.; Thomas, J. M. *J. Chem. Soc., Chem. Commun.* **1996**, 1435−1436.
(40) De Luca, P.; Nastro, A. *Stud. Surf. Sci. Catal.* **1996**, *105*, 221−228.
(41) Engelhardt, G.; Michel, D. *High-Resolution Solid State NMR of Silicates and Zeolites*; John Wiley & Sons: New York, 1987.
(42) Frydman, L.; Harwood: J. S. *J. Am. Chem. Soc.* **1995**, *117*, 5367−5368.
(43) *UXNMR, Acquisition and Processing of NMR Data*; Bruker: Karlsruhe, Germany, 1991.

($-^1/_2$, $+^1/_2$) central transition was achieved using a soft 90° pulse of duration 9 μs. The phase cycling was designed to select only the desired pathway (0) − (± 3) − (0) − (−1). Rotor synchronization ($\nu_r = 14.925$ kHz) along t_1 was used to eliminate intense sidebands appearing along the MQ dimension. Typical accumulation involved 2048 (t_2) × 128 (t_1) values for ^{23}Na and ^{27}Al 3Q experiments. For each t_1 step, the number of scans was typically 240 and 2400 for 3Q MAS on ^{23}Na and ^{27}Al, respectively. A 2D Fourier transform with respect to t_1 and t_2 leads to pure absorption mode 2D spectra.

Computer Simulations of Slow MAS Spectra. The computer simulations of slow MAS spectra were carried out using the time domain rotational echo analysis of Maricq and Waugh.[44] For the simulations, the experimentally identified silicon resonances in distinct environments were considered together with their site occupancies.

The overall time domain response of the observed ^{29}Si magnetization is adequately described by summing the chemical shielding experienced by silicon nuclei located at distinct crystallographic positions. However, for the slow MAS experiments, the spectral resolution is sufficient to distinguish only three distinctly different silicon environments (Si_I, Si_{II}, and Si_{III}) in the case of ETS-10 and four (above three and the silicon environment with an aluminum neighbor) in the case of ETAS-10. Further distinction within each of these based on crystallographic nonequivalence could not be made from slow MAS spectra due to instrumental and signal-to-noise considerations. However, this is found to be sufficient for the complete sideband analysis to be made for these silicon environments and these form the basis for our further discussion.

We consider that only the anisotropic chemical shielding interaction contributes to the sideband intensities. This allows us to write, for free induction decay of a spinning solid,

$$G(t) = \sum_i \exp(i\omega_0\bar{\sigma}t) \sum_{\alpha,\beta,\gamma} \exp\{i\omega_0\delta \int_0^t \xi(t')\,dt'\} \qquad (1)$$

where

$$\xi(t') = C_1 \cos \omega_r t + S_1 \sin \omega_r t + C_2 \cos 2\omega_r t + S_2 + \sin 2\omega_r t$$

$$\delta = \sigma_{33} - \sigma_{11}$$

$$\bar{\sigma} = {}^1/_3 Tr(\boldsymbol{\sigma})$$

$$\eta = \frac{\sigma_{11} + \sigma_{33} - 2\sigma_{22}}{\sigma_{33} - \sigma_{11}}$$

The detailed definition of the modulation coefficients C_1, S_1, C_2, and S_2 may be found in ref 44. σ_{11}, σ_{22}, and σ_{33} are the principal elements of the chemical shielding tensor defined in the principal axis system and the summation "*i*" is over I-, II-, III-type silicons. The sideband intensities are governed by the anisotropy (δ) and asymmetry (η) of the chemical shielding, and these are determined from the analysis of the slow MAS spectra. It may be noted that the conventional assignment of chemical shielding tensors, namely $\sigma_{11} \le \sigma_{22} \le \sigma_{33}$, has been used and the asymmetry parameter η has a value between −1 and +1, the extreme values corresponding to axially symmetric tensors. Here, the Euler angles (α, β, and γ) define the orientation of the chemical shielding tensor of the *i*th silicon species in the MAS rotor frame which in turn is oriented at an angle $\cos^{-1}(1/\sqrt{3})$ with respect to the main magnetic field.

A powder averaging was done in the three-dimensional Cartesian space defined by the Euler angles (α, β, and γ), and using eq 1, the rotational echo was calculated by evaluating the integral over one rotor period ($0-2\pi/\omega_r$) for a series of equally spaced time intervals with the spacing chosen to give an adequate spectral width. The rotational echo was replicated over a 230-ms period to give the resultant free induction decay. This was subsequently convoluted with an exponential line broadening function before Fourier transformation to give the slow MAS spectra. The simulations were carried out on a personal computer using a program written in Fortran.

(44) Maricq, M. M.; Waugh, J. S. *J. Chem. Phys.* **1979**, *70*, 3300−3316.

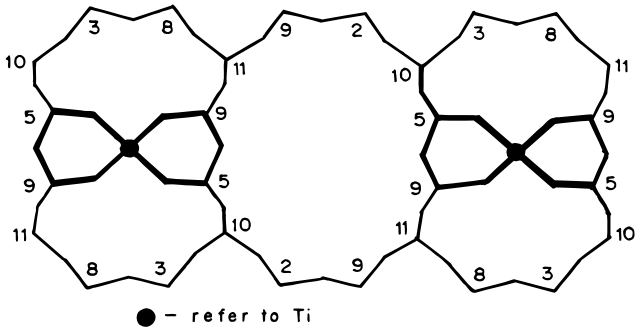

Figure 1. Computer graphics view of ETS-10 framework projected down the *c* axis showing the framework of Si and Ti atoms. The oxygens, lying approximately in the middle of the M atoms (where M = Si or Ti), are not labeled. For the numbering and connectivity of the M sites, please refer to Table 1. Atoms 1, 4, 6, and 7 occur in alternate layers below 10, 2, 5, and 5, respectively.

Table 1. Geometric Data of the Polymorph B of ETS-10 Structure

site (M)	M−O distance[a] (Å)	M−O−M angle[b] (deg)	connectivity[c]
Ti_1	1.887	145.990	Si_5, Si_5, Si_9, Si_9, Ti_3, Ti_3
Ti_2	1.887	144.687	Si_3, Si_3, Si_7, Si_7, Ti_3, Ti_3
Ti_3	1.883	145.340	Si_8, Si_6, Ti_1, Si_4, Ti_2, Si_2
Si_1	1.575	149.700	Si_4, Si_4, Si_7, Si_7
Si_2	1.577	142.820	Si_6, Si_9, Si_{10}, Ti_3
Si_3	1.577	142.652	Si_7, Si_8, Si_{10}, Ti_2
Si_4	1.577	144.352	Si_5, Si_8, Si_1, Ti_3
Si_5	1.577	143.447	Si_4, Si_9, Si_{10}, Ti_1
Si_6	1.580	143.147	Si_2, Si_{10}, Si_7, Ti_3
Si_7	1.580	142.507	Si_3, Si_1, Si_6, Ti_2
Si_8	1.577	145.140	Si_3, Si_4, Si_{11}, Ti_3
Si_9	1.577	143.762	Si_2, Si_5, Si_{11}, Ti_1
Si_{10}	1.577	150.772	Si_2, Si_3, Si_5, Si_6
Si_{11}	1.580	152.190	Si_8, Si_8, Si_9, Si_9

[a] The M−O distances are the average of six Ti−O distances for TiO_6 octahedra and the average of four Si−O distances for SiO_4 tetrahedra. [b] The M−O−M angles are the average of six Ti−O−M (where M = Ti or Si) angles for the TiO_6 octahedra and the average of four Si−O−M (where M = Ti or Si) angles for SiO_4 tetrahedra. [c] Neighboring M sites connected through bridging oxygen.

Molecular Modeling. The computer graphics (CG) visualization of ETS-10, the cluster model generation, and the semiempirical quantum chemical calculations were performed on a SiliconGraphics Indigo2 workstation using the Insight II software package[45] supplied by Biosym Technologies Inc. (U.S.). The ETS-10 lattice was modeled from the crystal structure reported by Anderson et al.[17,24] for the polymorph B. The unit cell of ETS-10 has a stoichiometry of $[M_{96}O_{208}]^{32-}$ (where M = Si or Ti), or precisely $[(SiO_2)_{80}(TiO_3)_{16}]$,$^{32-}$ where the Si/Ti ratio is 5.

A CG view of the ETS-10 framework showing the various Si and Ti sites is given in Figure 1. There are 11 distinct Si sites and three distinct Ti sites in the crystal structure of ETS-10 (polymorph B). All of the Ti sites are octahedrally coordinated, where two oxygen atoms are bridging to adjacent Ti sites and the remaining four oxygen atoms are bridging to Si sites. All of the Si sites are tetrahedrally coordinated, and there are basically two types of silicons; there are silicons [Si-(4Si)], where all the four oxygen atoms are bridging to adjacent Si sites, and silicons [Si(3Si,1Ti)], where three oxygen atoms are bridging to adjacent Si sites and the remaining oxygen atom bridging to adjacent Ti sites. The average M−O distances and M−O−M angles (where M = Si or Ti), calculated from the reported crystal structure, are given in Table 1. Semiempirical quantum chemical calculations using standard MNDO procedure were carried out on cluster models representing the Si sites in ETS-10 to understand the electronic structure, preferred locations for Al substitution, and resulting acidity.

(45) *Insight II user Guide*, Version 2.3.5; Biosym Technologies: San Diego, CA, 1994.

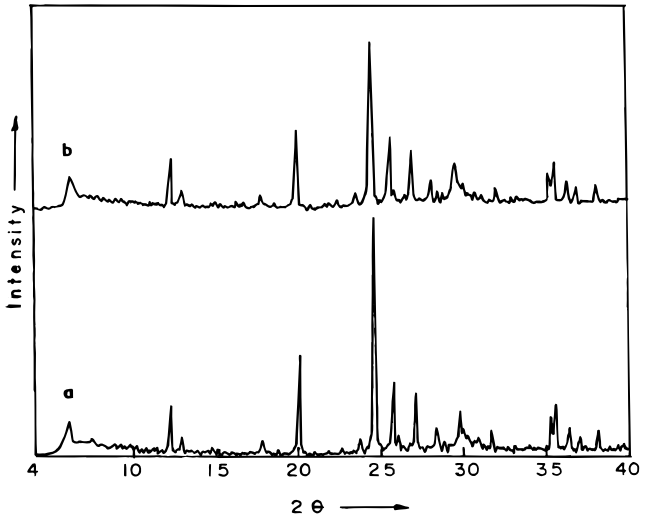

Figure 2. X-ray diffraction patterns obtained on (a) ETS-10 and (b) ETAS-10 synthesized as outlined in the text. The narrow reflections are readily indexed to the known structure of the highly crystalline ETS-10 phase, while the small broad feature is attributable to a possible stacking disorder in the structure.

Results and Discussion

The identification of the crystalline phase of the material and its exceptional phase purity were verified by XRD (Rigaku, Model D-max III). The diffraction pattern, shown in Figure 2 (as-synthesized), exhibits both broad and sharp reflections, as noted by Anderson et al.,[24,33] indicating that the material is highly crystalline exhibiting disorder. The XRD patterns in the range $2\theta = 4-40°$ could be indexed to the ETS-10 structure,[17,25,33−35,39] and the absence of impurity peaks shows that a highly crystalline ETS-10 and ETAS-10, devoid of the ETS-4 phase, has been synthesized. The diminished intensity of the peaks in the low-2θ region is attributable to occluded water.

^{29}Si MAS NMR Spectra of ETS-10. The ^{29}Si MAS NMR spectrum of ETS-10, referenced to tetramethylsilane, is shown in Figure 3a (here, a resolution enhancement using a suitable window function was carried out by apodizing the time domain NMR data with the UXNMR software package to enhance the spectral resolution). There is a noticeable absence of signal in the region around 90.0 ppm which confirms the absence of ETS-4 impurity and also the absence of silicon environment corresponding to [SiOH, $Si(OH)_2$] or the defect sites. Thus, the NMR results show that the synthesized material exhibits exceptional phase purity with the absence of defect sites.

The spectrum in Figure 3a shows three types of distinct silicon environments. The resonances (δ) due to the titanium-rich [Q^4-(3Si,1Ti)] (−94 to −95 ppm; −96 to −97 ppm) and silicious [Q^4(4Si,0Ti); −103 to −104 ppm] environments are readily identified and marked as I, II, and III, respectively, for further discussion. The observed spectrum could be deconvoluted into seven resonances as shown in Figure 3b, whose chemical shifts and peak areas can be measured accurately for quantitative analysis. The results are given in Table 2.

The approximate ratio of the intensity of the signals of I, II, and III sites is 4:4:2, which is in correspondence with the earlier reports.[17,24] In ETS-10, among the 11 crystallographically distinct Si sites, Si_1, Si_{10}, and Si_{11} are of the type III, namely Si(4Si,0Ti). Si_1 and Si_{11} have half-occupancy compared to the full occupancy of Si_{10}. Each of the two signals of equal intensity of type III Si sites can be assigned to $Si_1 + Si_{11}$ and Si_{10} or vice versa. This distinction within type III Si sites was not reported earlier probably due to poor spectral resolution.[17,24]

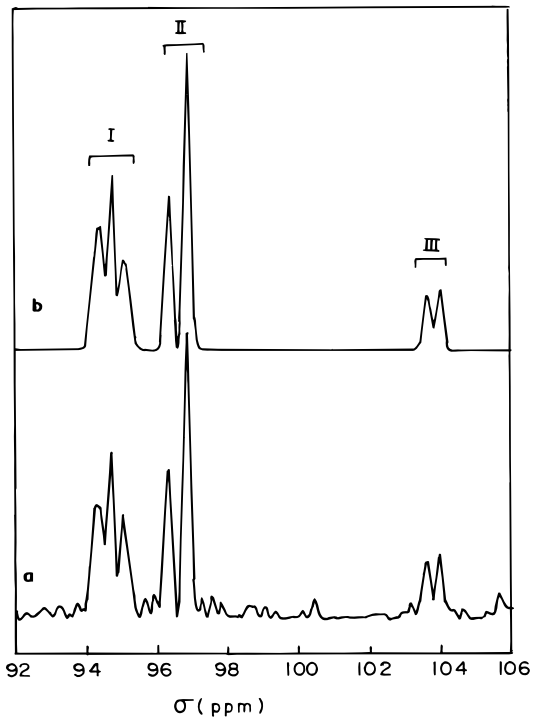

Figure 3. (a) Resolution-enhanced ^{29}Si MAS NMR spectrum of ETS-10 showing the distinct resonances corresponding to Si(4Si,0Ti) and two types of Si(3Si,1Ti), environments. (b) Simulation of spectrum (a) using a Gaussian function.

However, we could clearly distinguish two silicon resonances at −103.6 and −103.9 ppm (Figure 3a) with almost 1:1 intensity. The exact assignment of these resonances to the silicon sites could not be made because of the large deviation in M−O−M angles (see later).

The signals due to type I and II Si sites have been classified into four distinct types, namely A, B, C, and D, by Anderson et al.[17,24] This classification was based on their location in a 12-ring or 7-ring. However, an inspection of the structure shows that all Si sites have locations common to 12- and 7-rings. From the CG analysis of the topography of these silicon sites, we observe that there are two types of silicons, with respect to their coordination to titanium; Si_2, Si_4, Si_6, and Si_8 are coordinated to Ti_3, whereas Si_3, Si_5, Si_7, and Si_9 silicons are coordinated to either Ti_1 or Ti_2. Two distinct sodium ions, which balance the two negative charges on titanium, with different quadrupole tensors have been reported.[24] This points to possible occurrence of two different types of exchangeable cations corresponding to (Ti_1 or Ti_2) and (Ti_3) and suggests that type I and II [Si(3Si,1Ti)] sites could be classified on the basis of the titanium coordinated to it. However, our NMR results on ETAS-10 and molecular modeling rule out this possibility. This is discussed below.

^{27}Al and ^{29}Si MAS NMR of ETAS-10. The ^{27}Al MAS NMR spectrum of ETAS-10, synthesized in a typical Si/Al ratio of 42, is shown in Figure 4a. Tetrahedral framework incorporation of Al is borne out in Figure 4a by a very intense resonance at = 57.3 ppm. The presence of a weak signal at the octahedral Al position (∼0 ppm) is more clearly visible in the ^{27}Al MQ-MAS study and is attributable to occluded aluminum oxide in the pores.

The ^{29}Si MAS NMR spectrum of ETAS-10 (Si/Al = 42) is shown in Figure 4b. While type I, II, and III environments noticed in ETS-10 are seen to be retained in ETAS-10, additional resonances at −90.2 and −92.0 ppm appear. The loss of

Table 2. ^{29}Si Peak Positions and Relative Intensities of ETS-10 and ETAS-10

sample	property	type I	type II	type III	additional peaks[a] A	additional peaks[a] B
ETS-10	peak positions[b]	−94.1, −94.5, −94.7	−96.1, −96.6	−103.6, −103.9		
	relative intensity[c]	3.9 (1.7:1.3:0.9)	4.1 (1.8:2.3)	2.0 (1:1)		
ETAS-10; Si/Al = 42	peak positions	−93.9	−96.0	−103.5	−90.2	−92.0
	relative intensity	3.0	3.6	1.4	1.7	0.3

[a] Due to Si[2Si,1Ti,1Al] corresponding to Al substitution at Si (see text). [b] Peak positions (δ) are given in ppm with reference to TMS. [c] Values in parentheses denote integrated intensities of peaks resolved in each type.

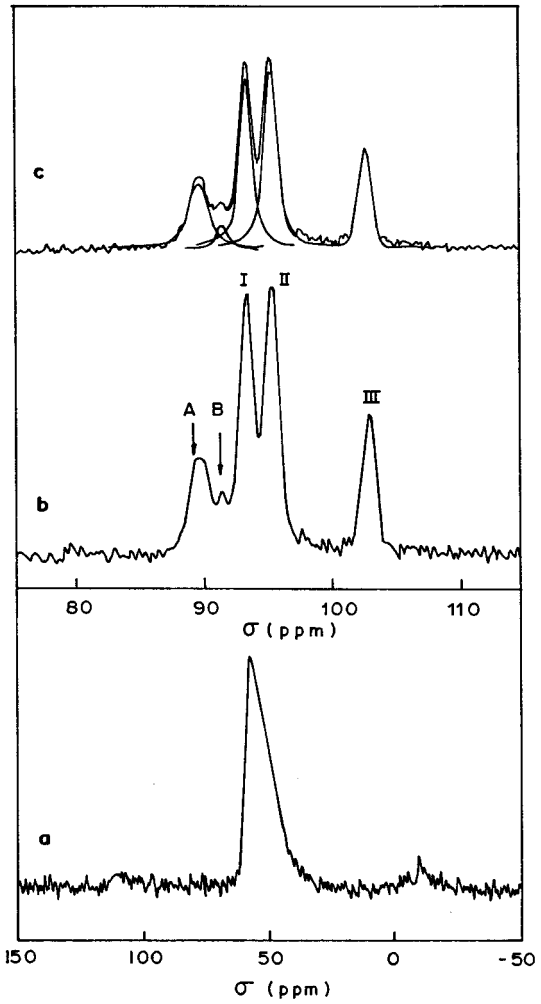

Figure 4. (a) ^{27}Al MAS NMR spectrum of ETAS-10 (Si/Al = 42). (b) ^{29}Si MAS NMR spectrum of ETAS-10 (Si/Al = 42). (c) Deconvoluted ^{29}Si MAS NMR spectrum of ETAS-10 (Si/Al = 42).

resolution due to peak broadening of the silicon resonances is observed in Figure 4b, compared to that in Figure 3, due to the incorporation of Al in the framework. The increased broadening is attributable to second nearest neighbor effects through the dipolar interactions between the spin-$^1/_2$ ^{29}Si nucleus and the spin-$^5/_2$ ^{27}Al nucleus, not eliminated in MAS experiments due to nonvanishing electric field gradients at the aluminum sites.[46] This is especially aggrevated at our 7.1-T field of operation. Deconvolution assuming a Gaussian-type peak function were performed with UXNMR software package. The deconvoluted spectrum was simulated, and the chemical shift values as well as the peak areas of these signals were calculated for quantitative analysis (Table 2).

It is known that Al substitution in various zeolite structures gives rise to a deshielding of ∼4.00 ppm for each Si substituted by Al.[41] This would imply that the new resonances in ETAS-10 samples arise from lattice substitution corresponding to an environment where Si coordinates to a titanium and aluminum. That this occurs in the neighborhood of type I and II sites would imply a preferential substitution of Al at the siliceous Si[4Si,0Ti] environments and hence an Al−Ti avoidance,[27,33] as clearly indicated in our studies. Among the two new peaks, the resonance at −90.2 ppm is more intense and arises from a preferential substitution of Al at the completely silicious site which is adjacent to site I. We rule out the possibility that this peak is due to ETS-4 impurity as we find that the peak intensity increases with increasing Al substitution and, further, the XRD data shows an absence of the impurity of ETS-4 phase. Similarly, the less intense peak at −92.0 ppm is due to Al substitution adjacent to site II. Quantum chemical calculations pinpoint the topographical location of the preferred silicon site for Al substitution and allow us to make further T-site assignments of I and II in ETS-10.

^{29}Si Slow MAS NMR and Disruption of Local Symmetry. Å striking feature of the ^{29}Si MAS spectrum of ETS-10 is the revelation of an intense and characteristic sideband pattern when the sample was spun at much slower speeds, namely ∼385 and 700 Hz. Typical spectra at these two spinning speeds are presented in Figure 5, parts a and b, respectively. This is in contrast to the spectrum taken at moderate spinning speeds (2.5−3.5 kHz, Figure 3) where the presence of spinning sidebands can be hardly noticed. The sideband pattern of signals of silicons of type I and II are quite similar, whereas type III is nearly sideband free, showing that the anisotropic chemical shielding at the siliceous and titanium-rich environments are markedly different.

The sideband intensities for the resonance at −103.9 ppm fall off very rapidly; a near-isotropy for the chemical shielding is readily discerned for the set of two resonances which were identified as $Si_1 + Si_{11}$ and Si_{10}. Our observations of very near isotropic nature of chemical shielding therefore reaffirm the earlier contention[17,24] that the set of resonances occurring in the −103.6 to −103.9 ppm range arises purely from siliceous environments devoid of any Si−O−Ti linkage, as only a central silicon connected tetrahedrally to four other lattice silicons can present a nearly perfect T_d symmetry for the chemical shielding. These are further supported from computer simulations of the slow MAS spectra shown in Figure 5c,d. A silicon in an isolated perfect tetrahedral environment of four more silicons has a T_d symmetry, and the chemical shielding tensor is spherically symmetric; the shielding anisotropy therefore vanishes by definition. The observation of the near-isotropy for chemical shielding reinforces our view that, while the tetrahedral arrangement of the siliceous environment is preserved, the slight distortions in the T-site geometry cause the tensor to slightly deviate from being isotropic, thus causing a slight anisotropy, albeit small, to be introduced. This is precisely the reason an empirical correlation of the T-site geometrical parameter, such as, for example, the T−O−T angle, with ^{29}Si chemical shifts

(46) Naito, A.; Ganapathy, S.; McDowell, C. A. *J. Magn. Reson.* **1982**, *48*, 367−381.

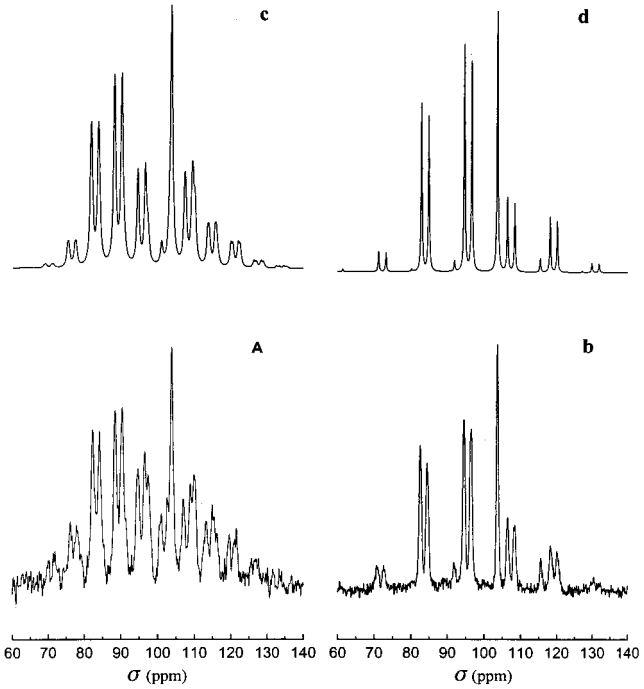

Figure 5. ^{29}Si slow MAS NMR experimental spectra of ETS-10, when the sample was spun at (a) 385 Hz and (b) 700 Hz. The corresponding computer-simulated spectra c and d are also shown above the experimental spectra. The additional splitting in sideband profile in spectrum a, especially for the type I and II resonances, is due to somewhat inferior spinner stability (±25 Hz) and is partly accounted for in the simulation. An exponential line broadening of 60 Hz was used in the simulations.

have been found.[47] In other words, the anisotropic shielding at each distinct Si site in the siliceous environment varies in a manner that is purely dictated by the extent of deviation from an ideal tetrahedral symmetry and has a direct bearing on the shielding tensor. This, in turn, causes the isotropic shift to change as well, thus giving rise to multiplicity of silicon resonances in the MAS spectra of highly siliceous zeolites.[48,49] Thus, the precise correspondence between structure and electronic shielding emerges as a consequence of bond geometry distortions in an ordered zeolite framework obeying a particular space group symmetry.

The intense spinning sidebands for the silicon resonances at ∼−94.5 and −96.5 ppm lend themselves for an immediate analysis. Computer simulations of the slow MAS spectra (Figure 5c,d; see also Table 3) show that the silicon environment is characterized by an anisotropic chemical shielding tensor with the principal elements σ_{11} and σ_{22} being equal in magnitude and σ_{33} distinct. The chemical shielding at I and II is therefore axially symmetric, and unmistakably, there is a transformation from a near-T_d symmetry to C_{3v} symmetry. A Si environment which has three silicons and one titanium as bridged neighbors would make this symmetry transformation possible. Our observations therefore conclusively show that Si[3Si,1Ti] type silicons occur in ETS-10 and further confirm earlier assignment of the silicon signals at −94.6 and −96.6 ppm to these type of silicons. On the basis of symmetry considerations, the 3-fold rotational axis of symmetry will be along the Si−Ti vector. An inspection of the X-ray-determined structure of ETS-10 shows the presence of a chain of −Ti−O−Ti− which connects all of the titanium octahedra. From the connectivity between SiO_4 tetrahedra and TiO_6 octahedra, the orientation of the unique C_{3v} axis of the chemical shielding tensor of Si[3Si,1Ti] is perpendicular to the long −Ti−O−Ti− chains.

Table 3. Anisotropic ^{29}Si Chemical Shielding Parameters[a] for ETS-10 and ETAS-10

sample	type	σ_{11}[b]	σ_{22}[b]	σ_{33}[b]	$\bar{\sigma}$[b]	δ[b]	η[b]
ETS-10[c]	I	79.8	79.8	124.5	94.7	44.7	1.0
	II	81.8	81.8	126.5	96.7	44.7	1.0
	III	94.0	108.1	109.0	103.7	15.0	−0.9
ETAS-10[d]	I	79.5	79.5	125.0	94.7	45.5	1.0
	II	81.5	81.5	127.0	96.7	45.5	1.0
	III	94.0	108.2	109.0	103.4	15.0	−0.9
	A, B	75.5	76.5	121.0	90.8	45.5	1.0

[a] Values in ppm with respect to TMS. Positive values (in σ scale) denote increasing shielding. I, II, III, and (A, B) refer to the silicon environments as discussed in the text. [b] For definition see text. [c] From 700-Hz slow MAS computer simulations. [d] From 645-Hz slow MAS computer simulation.

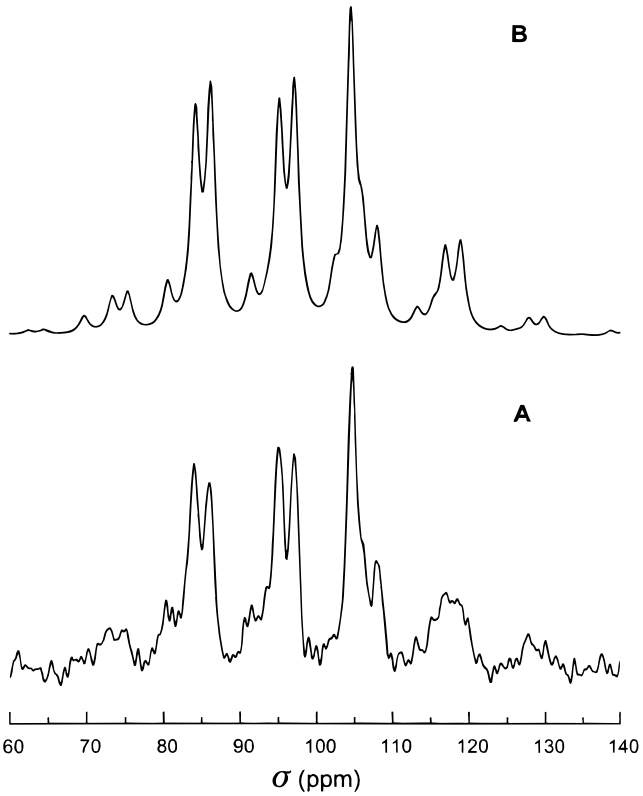

Figure 6. ^{29}Si slow MAS spectrum (A) of ETAS-10 (Si/Al = 62) when the sample was spun at 645 Hz. (B) corresponding computer-simulated spectrum. An exponential line broadening of 260 Hz was used in the simulations.

The analysis of the slow MAS spectra of ETAS-10 (Si/Al = 42) was carried out as before, and these results are also collected in Table 3. The corresponding spectral simulations are shown in Figure 6. For this simulation, four distinct Si environments shown in Figure 4b were considered (I, II, III, and A). The peak B is not resolved under low spinning because of increased broadening. Three of them correspond to Si sites belonging to types I, II, and III, as in the parent ETS-10 structure, while the fourth one, belongs to Si[2Si,1Ti,1Al]. Despite the small differences in the simulated intensities obtained, the spectra could be simulated using the anisotropy and asymmetry parameters found for ETS-10. The chemical shielding tensors for Si sites of types I, II, and III are completely preserved in the ETAS-10 structure, thus ensuring identical or near-identical

(47) Ramdas, S.; Klinowski, J. *Nature* **1984**, *308*, 521−523.
(48) Radeglia, R.; Engelhardt, G. *Chem. Phys. Lett.* **1985**, *114*, 28−30.
(49) Fyfe, C. A.; Grondey, H.; Feng, Y.; Kokotailo, T. *J. Am. Chem. Soc.* **1990**, *112*, 8812−8820.

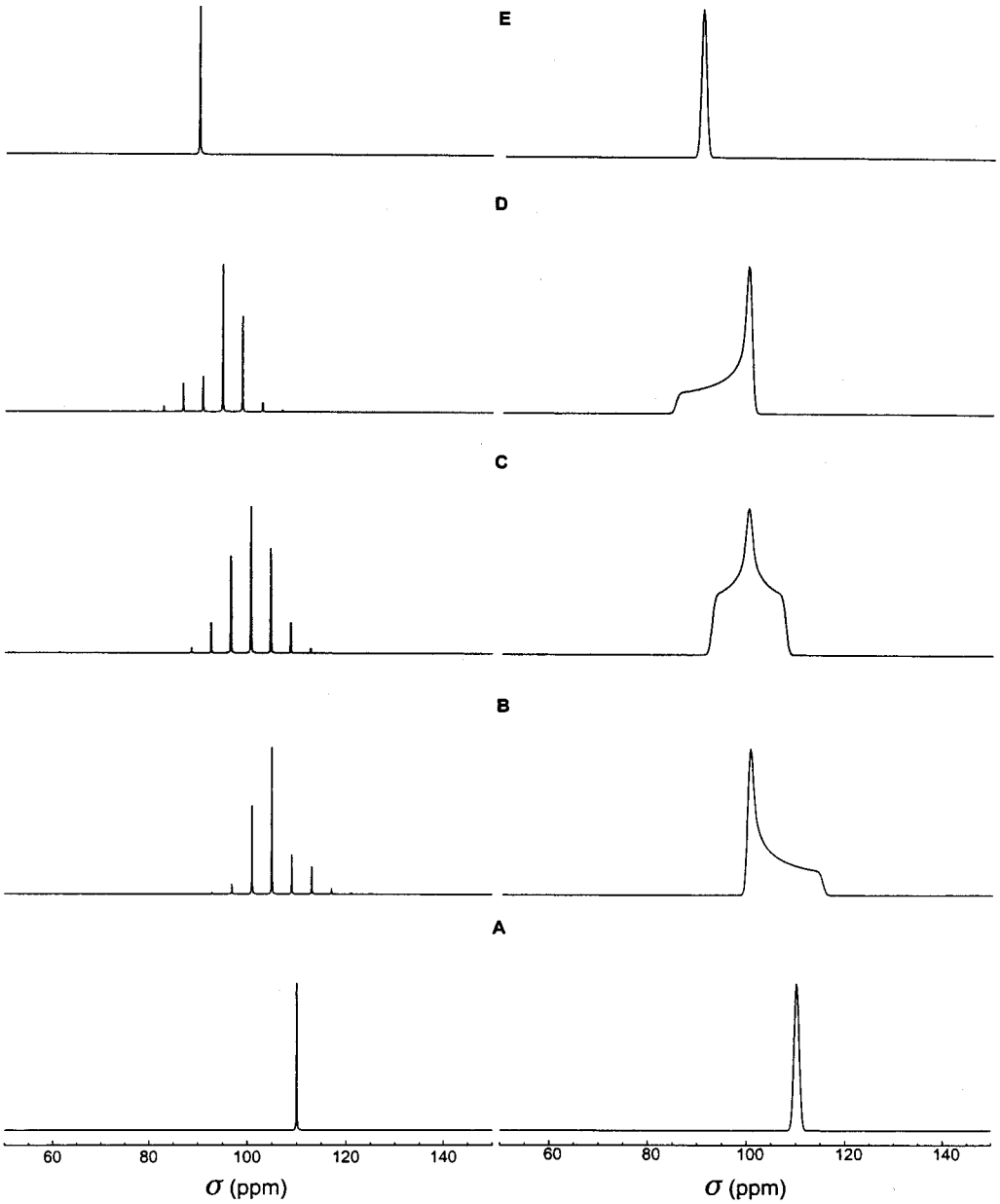

Figure 7. Computer simulations of ^{29}Si slow MAS spectra at a representative spinning speed of 400 Hz to show the correspondence between the change in local symmetry due to heteroatom (M) substitution and the ^{29}Si chemical shielding (A) Si(4Si,0M); (B) Si(3Si,1M); (C) Si(2Si,2M); (D) Si(1Si,3M); (E) Si(0Si,4M). The Gaussian broadened static spectra are also shown side by side. Spectral simulations were carried out using $\delta =$ 15 ppm (B, C, and D). A downfield isotropic shift of 5 ppm for every M substitution has been considered in the simulations.

T-site geometries for these sites in the structures of Al-substituted materials. The additional sideband pattern noticed for the Si[2Si,1Ti,1Al] environment also fits to an axial tensor. It is probable that Al substitutes the Si site isomorphously without disturbing the T_d coordination of the T site. However, the geometry varies in such a way that the heteroatom substitution causes the net isotropic shift to change by as much as 5 ppm, and yet, this environment possesses a overall C_{3v} symmetry for the electronic shielding, considering the presence of one neighboring Ti site.

Our approach has general utility in resolving disputes in all zeolite lattices where heteroatoms are isomorphously substituted in place of Si. The stepwise substitution by a heteroatom (M) would transform the local symmetry in the order T_d (0M) $\rightarrow$ C_{3v} (1M) $\rightarrow$ C_{2v} (2M) $\rightarrow$ C_{3v} (3M) $\rightarrow$ T_d (4M) as the extent of substitution increases. As an aid to this generalization of the slow MAS approach for isomorphic heteroatom substitutions, we show in Figure 7 the computer simulated slow MAS and static ^{29}Si spectra for generic representations of lattice substitution by none [Q^4(4Si,0M)](A), one [Q^4(3Si,1M)](B), two [Q^4-(2Si,2M)](C), three [Q^4(1Si,3M)](D), and four [Q^4(0Si,4M)](E) heteroatoms (M), and these serve to indicate that indeed the change in local symmetry has a great influence on the ^{29}Si chemical shielding which can be conveniently monitored at high superconducting magnetic fields.

Molecular Modeling Studies. MNDO (modified neglect of differential overlap) calculations were performed to compute the energies of substitution of a single aluminum atom in place of silicon in the ETS-10 framework leading to ETAS-10. The preferred site of aluminum substitution and its consequences on the acidic properties of ETAS-10 are also studied. The geometry of a typical cluster model representing the crystallographic site Si_{10} is shown in Figure 8. Similar cluster models are derived for the other sites in ETS-10 from the reported crystal structure of polymorph B. A cluster containing one tetrahedral group, namely $Si(OH)_4$ (denoted as monomer), is

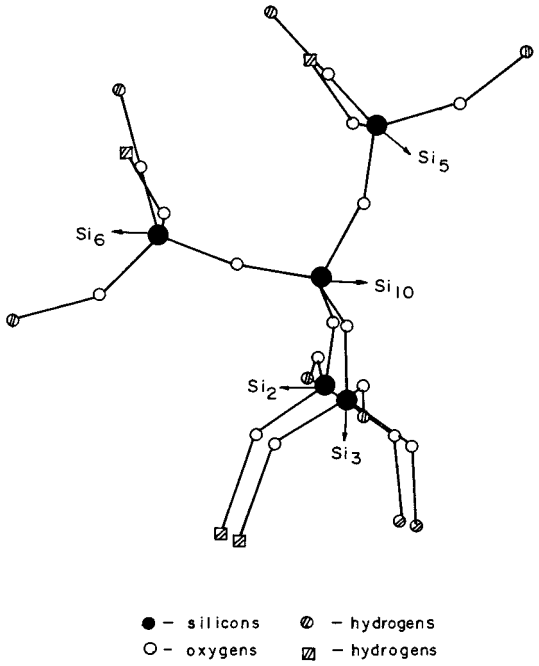

Figure 8. Computer graphics picture of the cluster model chosen to study the electronic property of Si_{10} site. Hydrogens marked as squares represent neighboring Ti sites, while hydrogens marked as circles represent neighboring Si sites.

considered for studying the electronic properties. The terminal oxygen atoms of SiO_4 group are bonded to hydrogen atoms to maintain the electrical neutrality of the cluster. The positions of these terminal hydrogen atoms are located at the nearest-neighbor M-site (where M = Si or Ti) locations.

A larger pentamer cluster model was generated to study the aluminum substitution process. The pentamer cluster model $\{SiO_4[Si(OH)_3]_4\}$ represents a SiO_4 group which shares the corners with four adjacent SiO_4 groups through bridging oxygen atoms. Such pentameric cluster models were generated for the Si sites of type III, namely Si_1, Si_{10}, and Si_{11}, since our MAS NMR studies conclusively showed that these are the sites where Al substitution occurs. The process of substitution of aluminum in ETS-10 lattice is considered as follows:

$$SiO_4[Si(OH)_3]_4 + [Al(OH)_4]^- \rightarrow AlO_4[Si(OH)_3]_4^- + Si(OH)_4 \quad (2)$$

The substitution energy (SE) of aluminum for silicon in the above process is calculated from their total energies (TE) according to the equation

$$SE = TE_{products} - TE_{reactants} \quad (3)$$

The acidity is studied by compensating the negative charge in the $AlO_4[Si(OH)_3]_4^-$ cluster by adding a hydrogen to the bridging oxygen between Al and Si. Although there are four possible bridging oxygens, the hydrogen is attached to the bridging oxygen which is facing the large 12-member ring of the ETS-10 lattice. The binding energy of the proton (BE_H) is calculated by considering the following process:

$$AlO_4H[Si(OH)_3]_4 \rightarrow AlO_4[Si(OH)_3]_4^- + H^+ \quad (4)$$

and the following relation:

$$BE_H = TE(AlO_4H[Si(OH)_3]_4) - TE(AlO_4[Si(OH)_3]_4^-) \quad (5)$$

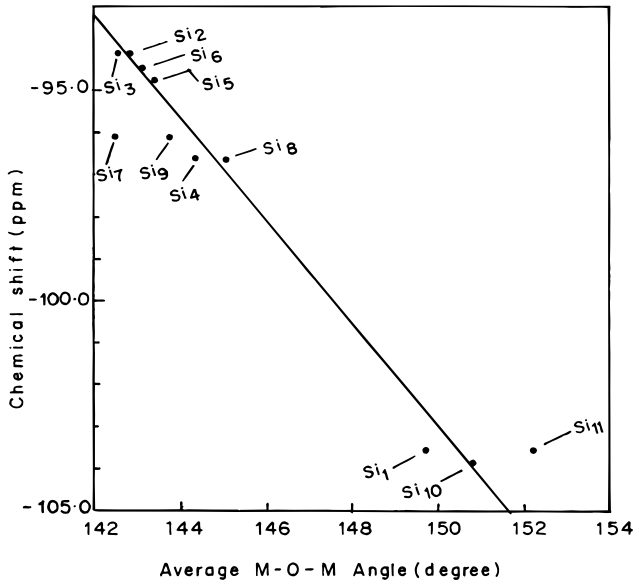

Figure 9. Assignment of crystallographically nonequivalent Si sites based on their chemical shift correlation with the M−O−M angles derived from X-ray structure of ETS-10.

Table 4. Energetics Derived from Quantum Chemical Calculations for Various Cluster Models Representing the Sites Si_1, Si_{10}, and Si_{11}

cluster site	cluster model	total energy (eV)	relative aluminum substitution energy (eV)	relative proton binding energy (eV)
1	$Si(OH)_4$	−3816.80		
10	$Si(OH)_4$	−3815.22		
11	$Si(OH)_4$	−3813.56		
1	$[Al(OH)_4]^-$	−3562.40		
10	$[Al(OH)_4]^-$	−3560.86		
11	$[Al(OH)_4]^-$	−3559.23		
1	$SiO_4[Si(OH)_3]_4$	−5724.73		
10	$SiO_4[Si(OH)_3]_4$	−5724.45		
11	$SiO_4[Si(OH)_3]_4$	−5724.20		
1	$AlO_4[Si(OH)_3]_4^-$	−5682.55	−0.15	−0.31
10	$AlO_4[Si(OH)_3]_4^-$	−5682.85	−0.69	0.00
11	$AlO_4[Si(OH)_3]_4^-$	−5681.94	0.00	−0.69

The cluster site, the cluster model and total energy of the clusters are given in Table 4. The substitution energy evaluated according to eq 3 for process 2 at the three possible sites are also given in Table 4. The substitution energy of aluminum at the Si_{10} site is the most favorable and hence preferential substitution at Si_{10} is expected. When Si_{10} is substituted by aluminum, the silicons adjacent to Si_{10}, which are Si_2, Si_3, Si_5, and Si_6, are expected to undergo a downfield shift by 4 ppm, as is indeed observed. With this, the resonances of type II silicons could be assigned to Si_4, Si_7, Si_8, and Si_9.

In earlier reports,[47−49] it has been shown that there is a linear correlation between the NMR chemical shifts and the Si-site geometry, namely the average Si−O−Si angle. We derived the Si−O−Si angle for all the 11 sites from the structural report and then plotted against the experimental chemical shift. However, when more than one peak could not be deconvoluted, the average Si−O−Si angles were considered. Our assignment is further testified from the plot of chemical shift versus M−O−M angle as shown in Figure 9, which shows almost a linear variation.

The slight deviations noticed in T-site correlation are thought to arise from the influence of other geometrical parameters such as M−O distances, O−M−O angles, and O−M−O−M dihedral angles. It may also be noted that the signals for the eight silicons

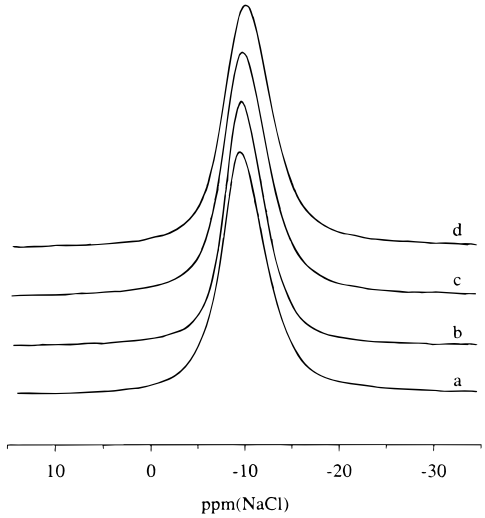

Figure 10. 105.8-MHz ^{23}Na MAS spectra of ETS-10 (a) and ETAS-10, Si/Al = 62 (b), 42 (c), and 22 (d).

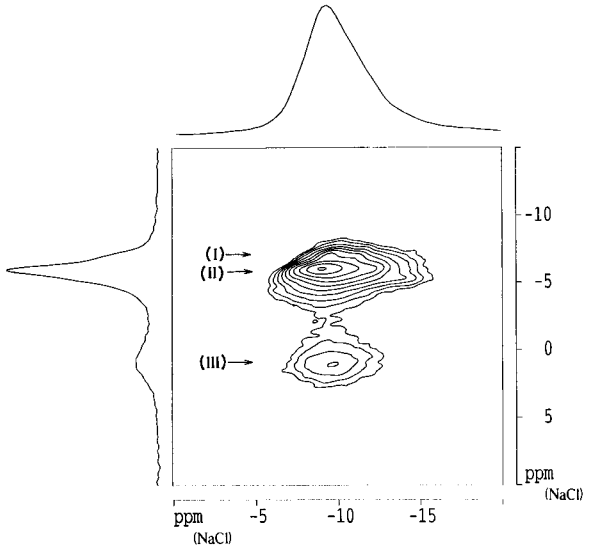

Figure 11. 105.8-MHz ^{23}Na 3Q MAS spectrum showing the resolution of cation sites in ETS-10. The labels (I), (II) and (III) correspond to the different sodium environments as discussed in the text.

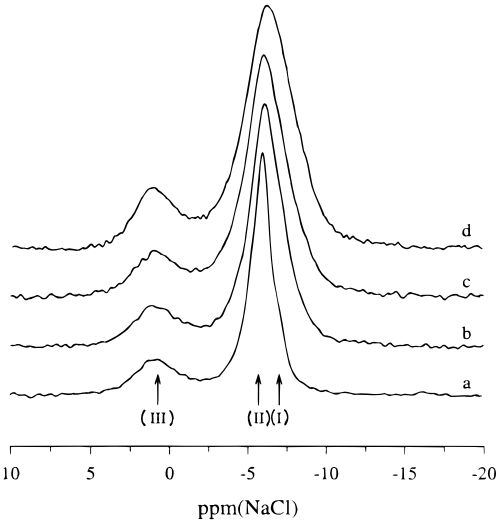

Figure 12. Isotropic projection of ^{23}Na 3Q MAS spectra of ETS-10 (a) and ETAS-10, Si/Al = 62 (b), 42 (c), and 22 (d). These spectra were obtained by a projection of the sheared 2D data sets as mentioned in the text.

of type I and type II lie in rather restricted chemical shift range −94.1 to −96.6 ppm. Further enhancement in chemical shift dispersion may become noticeable at very high magnetic fields.

The cations compensating the anionic framework charge due to aluminum substitution can be protons and they impart Bronsted acidity. The binding strength of protons to the oxygen atoms bridging silicon and aluminum is an indication of acid strength. We have evaluated the acidity of protons bonded to different oxygen sites, by calculating the proton binding energy according to eq 5. It is observed that the site where most facile substitution of aluminum occurs, namely Si_{10}, creates the stronger acidity. As predicted by the proton binding energy, the proton is weakly bound, when Al substitutes Si_{10} (Table 4).

^{23}Na and ^{27}Al MQ-MAS NMR. Recently, a new 2D MQ-MAS experiment on quadrupolar nuclei was proposed by Frydman and Harwood[42] and further developed by Fernandez and Amoureux.[50,51] Since this method completely averages out anisotropic interactions, such as dipolar and chemical shieldings, as well as second-order quadrupolar broadening, it gives new access for studying half-integer quadrupolar nuclei, such as the sodium cations and the aluminum sites in molecular sieves. In this experiment, an isotropic spectrum of the quadrupolar nucleus can be obtained from 2D correlation of 3Q (or 5Q in ^{27}Al) and 1Q transitions. Separation of contributions from quadrupole interactions and chemical shieldings is readily achieved, and one can get valuable information about the distribution of CS of nonequivalent sites and further of the electric field gradients at these sites. Our application of this method to ETS-10 and ETAS-10 is also the first attempt to characterize the cation environment in molecular sieves by MQ-MAS NMR.

In ETS-10 and ETAS-10, sodium cations partly counterbalance the negative framework charge due to octahedrally coordinated titanium. Simple ^{23}Na MAS spectra of ETS-10 and ETAS-10, shown in Figure 10, are featureless, and no information can be discerned about the cation environments. All spectra display single asymmetric lines devoid of quadrupolar features. Although the second-order quadrupole broadening of the observed ($-^1/_2$, $+^1/_2$) central transition is less severe at the high-field (9.4-T) operation, no clue about the cation site distribution is available from those spectra. In ETAS-10 samples, there is an increasing broadening with increasing aluminum substitution (Figure 10,b−d).

3Q-MAS correlation experiments were performed on ETS-10 and ETAS-10 using a three-pulse sequence as discussed in the Experimental Section. The result is shown in Figure 11 as a 2D contour plot for the 3Q-MAS experiment conducted on ETS-10. A shear transformation during 2D Fourier transform has been used to align the anisotropic (A) direction parallel to the δ_2 horizontal axis, so that a projection parallel to this axis gives rise to the isotropic (δ_{iso}) dimension and yields a high-resolution spectrum of sodium without second-order quadrupole broadening. The isotropic spectra so obtained on ETS-10 and ETAS-10 are compared in Figure 12. Several important aspects of MQ-MAS results are discussed below.

We recognize distinct sodium environments from the results presented in Figures 11 and 12. A careful inspection of the isotropic spectrum (Figures 11 and 12a) reveals three non-equivalent sodium sites in the structure of ETS-10. One of these sites is well-resolved, whereas two other sites have considerable

(50) Fernandez, C.; Amoureux, J. P. *Chem. Phys. Lett.* **1995**, *242*, 449−454.

(51) Fernandez, C.; Amoureux, J. P. *Solid State Nucl. Magn. Reson.* **1996**, *5*, 315.

3Q spectral overlap. The three sites are marked (I), (II), and (III) in the figure. A recourse to ETS-10 structure shows that the asymmetric unit contains three crystallographically nonequivalent titaniums, of which Ti_1 and Ti_2 are similar due to the silicon and titanium connectivities to their immediate neighbors, while site Ti_3 is distinct (see also connectivity Table 1). This is also noticed in the ^{29}Si MAS NMR spectrum, as discussed earlier. The charge-balancing role of the sodium cations at these distinct titanium sites is clearly borne out from our 3Q-MAS studies. Although for complete charge balancing we require two sodiums for each nonequivalent titanium, the observation of only three sodium sites from 3Q-MAS experiments suggests that sodium cations probably occupy symmetry-related positions so that the two sodiums on each titanium become pairwise equivalent. Indeed, such a picture emerges from cation modeling of sodium positions in ETS-10.[52] It is noticed that sodium ions coordinate to titanium atoms in such a way that they are located on either side of titanium and form a chain of sodium atoms that run almost parallel with Ti−O−Ti chains, the sodiums residing in the small pores built from 7-member rings. It is essentially sodium-rich, and the presence of potassium ions at low concentration is not likely to alter our conclusions about sodium environments derived from MQ-MAS NMR studies.

The expected 2:1 relative intensity of site (I, II) to site (III) is not readily apparent in the isotropic spectra of Figures 11 and 12. It is realized that sites (I, II) and (III) experience quadrupolar interaction of different magnitude. In the MQ-MAS experiment, sites with different quadrupolar interactions are not excited to the same extent for the generation of multiple-quantum coherences with the same efficiency. In particular, site (III), which experiences a much stronger quadrupolar interaction, develops weaker coherence compared to that for (I, II). However, by the knowledge of the rf field, especially of the multiple-quantum creation and conversion pulses, and also by the first estimate of C_q of each line, it is possible to stimulate the pulse response of the sites to a given experimental condition. The numerical method which involves the computation of the density matrix evolution under the rf power and spinning speed used in the experiment is fully described in ref 53. The result of this calculation is shown in Figure 13. The relative intensity found by this method is in remarkably good agreement with the expected 2:1 sodium site population.

The sodium sites are further characterized by C_q and δ_{CS}, which are the quadrupole interaction and isotropic chemical shift parameters, respectively. After shearing, the chemical shift axis is located with a slope of 1, while the QIS direction has a slope of −10/17. It is readily seen from Figure 11 that the two contours associated with (III) and (I, II) are displaced with respect to both of these axes so that they are characterized by different sets of quadrupolar and chemical shift parameters. An analysis of the 2D data gives an estimate of C_q and δ_{CS}, which are 0.9 MHz, −7 ppm and 1.65 MHz, −2.5 ppm for sites (I, II) and (III), respectively.

We show in Figure 12b−d the ^{23}Na 3Q MAS isotropic projection spectra for ETAS-10 with increasing aluminum substitution. These spectra are devoid of the second-order broadening and reveal distinct sodium sites whose peak maxima occur at the sum of the isotropic chemical shift and the quadrupole triple-quantum-induced shift.[54] When compared with the result obtained on ETS-10 (Figure 12a), it is clear that the sodium environments are intact in the aluminum-substituted materials, except for the additional broadening. This broadening is seen to increase with increasing aluminum content, and the distinction of (I) and (II) type environments is quickly lost. It may also be noted that the site (III) position is unchanged. The ^{29}Si MAS NMR results discussed earlier show that the framework structure of the aluminum-substituted material conforms to parent ETS-10 structure. In addition, the present 3Q MAS observations in ETAS-10 show that the cation environment is unchanged as well. Taken together, our studies lend credence to the view that the overall structure of ETAS-10 is the same as that of ETS-10 and that the heteroatom substitution occurs isomorphically. We believe that the observed broadening arises mainly from a distribution of isotropic chemical shifts and is only slightly due to a distribution caused by quadrupolar effects, since the 2D contour plots show distorted patterns with ridges that extend along the diagonal of slope 1.

In an effort to characterize the tetrahedrally substituted aluminum sites by MQ-MAS NMR, we have performed the 3Q MAS experiments for the $I = {}^5/_2$ aluminum nuclei in ETAS-10 with different Si/Al. The triple-quantum−single-quantum cor-

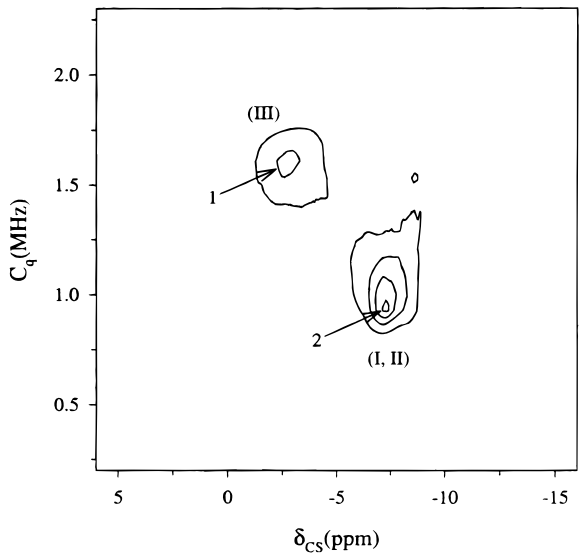

Figure 13. Quantification of the experimentally determined sodium sites (I, II) and (III) in ETS-10. This is obtained by a computer simulation of the actual response on the experimentally observed 2D data matrix to give the indicated population numbers as well as the quadrupole (C_q) and chemical shift (δ_{CS}) parameters.

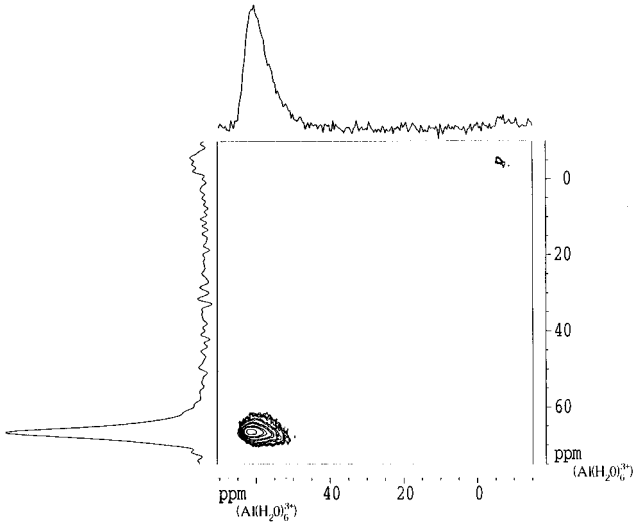

Figure 14. 104.3-MHz ^{27}Al 3Q MAS spectrum of ETAS-10 (Si/Al = 22). The intense contour is due to tetrahedral framework aluminum.

In an effort to characterize the tetrahedrally substituted aluminum sites by MQ-MAS NMR, we have performed the 3Q MAS experiments for the $I = {}^5/_2$ aluminum nuclei in ETAS-10 with different Si/Al. The triple-quantum−single-quantum cor-

(52) Yang, X.; Blosser, P. W. *Zeolites* **1996**, *17*, 237−243.
(53) Zwanziger, J. W. *Solid State Nucl. Magn. Reson.* **1994**, *3*, 219.
(54) Medek, A.; Harwood: J. S.; Frydman, L. *J. Am. Chem. Soc.* **1995**, *117*, 12779−12787.

relation is shown as a 2D contour plot in Figure 14 for Si/Al = 22. Despite the low Al loading, presence of octahedral aluminum is clearly visible in the 2D plot. Similar spectral features were noticed in other samples with increasing Si/Al. A feature of the 3Q MAS result is that the isotropic projection spectrum gives a much sharper resonance for the tetrahedral site at 65 ppm along the isotropic dimension, suggesting that a highly crystalline material has been synthesized. Within the resolution afforded by 3Q MAS, we however do not get any clue about the presence of nonequivalent tetrahedral aluminum sites. It is probable that the aluminum substitution occurs preferentially at the silicious environments, in the manner that molecular modeling studies show.

Conclusions

In this paper, we have presented a detailed analysis of the MAS NMR of highly pure ETS-10 and ETAS-10 molecular sieves which were synthesized without the use of any ETS-4 seeds. The ^{29}Si MAS NMR spectra at 7.1-T field display superior resolution and allow individual T sites to be recognized. A combination of NMR and molecular modeling is shown to be a very powerful approach for the exact location of Al substitution and the Bronsted acidic sites and the assignment of different tetrahedral silicon sites. The strategy involves isomorphic substitution of silicon by Al in ETS-10 lattice and Al substitution energy calculations by quantum chemical methods. We have also addressed the question of heteroatom lattice substitution in molecular sieves by slow MAS NMR. We show that this approach is very effective in establishing isomorphic substitution in molecular sieves through changes in chemical shielding tensor brought by transformation of local symmetry. This has been demonstrated in ETS-10 and ETAS-10. The power of the MQ-MAS NMR technique to determine the cationic sites occupied by sodium in ETS-10 and ETAS-10 is demonstrated.

Supporting Information Available: Tables of Si−O and Ti−O distances and Si−O−Si and Si−O−Ti angles in ETS-10 (2 pages, print/PDF). See any current masthead page for ordering information and Web access instructions.

JA972714O